Chronic cerebral hypoperfusion alters amyloid- peptide pools leading to cerebral amyloid angiopathy, microinfarcts and hemorrhages in Tg-SwDI mice

Chronic cerebral hypoperfusion alters amyloid-β peptide pools leading to cerebral amyloid angiopathy, microinfarcts and haemorrhages in Tg-SwDI mice

Natalia Salvadores[1, 2], James L. Searcy[1], Philip R. Holland[1, 3], and Karen Horsburgh[1, 4*]

[1]Centre for Neuroregeneration, University of Edinburgh, Chancellor's Building, 49 Little France Crescent. Edinburgh. EH164SB, UK.

[2]Center for Integrative Biology, Universidad Mayor, Chile

[3]Headache Group, Basic and Clinical Neuroscience, Institute of Psychiatry, Psychology and Neuroscience, King's College London, London, UK.

[4]Centre for Cognitive Ageing and Cognitive Epidemiology, University of Edinburgh, 7 George Square, Edinburgh, EH89JZ, UK.

*corresponding author karen.horsburgh@ed.ac.uk

Abbreviations:

amyloid-β (Aβ)

amyloid precursor protein (APP)

cerebral amyloid angiopathy (CAA)

NADPH Oxidase-2 (NOX2)

interleukin-1β (IL-1β)

transgenic mice with Swedish, Dutch and Iowa mutations in human APP (Tg-SwDI)

low density lipoprotein receptor-related protein (LRP)

receptor for advanced glycation endproducts (RAGE)

ABSTRACT

Cerebral hypoperfusion is an early feature of Alzheimer's disease (AD) that influences the progression from mild cognitive impairment to dementia. Understanding the mechanism is of critical importance in the search for new effective therapies. We hypothesised that cerebral hypoperfusion promotes the accumulation of amyloid-β (Aβ) and degenerative changes in the brain and is a potential mechanism contributing to development of dementia. To address this we studied the effects of chronic cerebral hypoperfusion induced by bilateral carotid artery stenosis on Aβ peptide pools in a transgenic mouse model of AD (Tg-SwDI) at an age when fibrillar amyloid burden is minimal. Cerebrovascular integrity was characterised by quantifying the occurrence of microinfarcts and haemorrhages and compared to wild-type mice without Aβ. A significant increase in soluble Aβ peptides (Aβ40/42) was detected after 1 month of hypoperfusion in the parenchyma in parallel with elevated amyloid precursor protein (APP) and APP proteolytic products. Following 3 months, a significant increase in insoluble Aβ40/42 was determined in the parenchyma and vasculature. Microinfarct load was significantly increased in the Tg-SwDI as compared to wild-type mice and further exacerbated by hypoperfusion at one and three months. In addition, the number of Tg-SwDI hypoperfused mice with haemorrhages was increased compared to hypoperfused wild-type mice. Soluble parenchymal Aβ was associated with elevated NADPH Oxidase-2 (NOX2) which was exacerbated by one month hypoperfusion. We suggest that in response to hypoperfusion, increased Aβ production/deposition may contribute to degenerative processes by triggering oxidative stress promoting cerebrovascular disruption and the development of microinfarcts.

Clinical perspective:

- Cerebral hypoperfusion influences the progression from mild cognitive impairment to dementia such as Alzheimer's disease.
- The mechanisms may involve promotion of amyloid production/deposition and degenerative changes (such as microinfarcts).
- NADPH Oxidase-2 may present a key target to protect against hypoperfusion-induced changes.

Introduction

Vascular risk factors have a major influence on age-related neurodegeneration and dementia [1]. Furthermore, it is now recognised that vascular dysfunction and cerebral hypoperfusion are evident in the early stages of Alzheimer's disease (AD) [2, 3]. The reduction in cerebral perfusion correlates with the severity of dementia and evidence from longitudinal epidemiological and neuroimaging studies suggest that underlying chronic cerebral hypoperfusion contributes to cognitive decline [3-5]. Regional alterations in brain perfusion may also predict those at risk of progression from mild cognitive impairment to dementia [4, 5].

The mechanism by which chronic cerebral hypoperfusion may lead to cognitive impairment is being explored through animal models. Our work, and others, has shown that cerebral hypoperfusion leads to cognitive decline through mechanisms that initially involve hypoxia-induced white matter injury, endothelial dysfunction, microvascular damage and a sustained pro-inflammatory response [6-11]. Prominent gliovascular damage and the development of vascular lesions (microinfarcts and haemorrhages) [10] are found with sustained hypoperfusion after several months.

Cerebral microinfarcts are a common finding in AD brains [12, 13] and linked to cerebral amyloid angiopathy (CAA) [14-18]. Additionally, microinfarction has been shown to occur regionally in areas of brain hypoperfusion in AD patients [19] and, as indicated, in models of cerebral hypoperfusion [10, 20]. Importantly, cerebral microinfarcts have been implicated as important contributors to cognitive impairment [21-23]. Although the mechanisms leading to microinfarct formation remain unknown, oxidative stress and inflammation, as the result of cerebrovascular alterations, have been suggested as possible contributors [24, 25]. NADPH

Oxidase-2 (NOX2) constitutes the main reactive oxygen species (ROS) source in the brain and it has a critical role in cell death following ischaemic insults [24-26]. Notably, mice lacking NOX2 develop significantly reduced infarct volumes following transient cerebral ischemia [26-28]. Moreover, NOX2 has been shown to be involved in post-ischaemic brain inflammation, which exacerbates the progression of brain injury [24].

Increasing evidence demonstrates an association between Aβ-induced neuronal damage and oxidative stress, which has been shown to involve microglial activation [29-34]. Aβ is able to increase the processing of pro-interleukin-1β (IL-1β) into mature IL-1β in microglia via increased reactive oxygen species [35]. In addition, transgenic amyloid protein precursor mice (TgAPP) lacking NOX2 showed improved cerebrovascular function and behavioral performance through reduction of oxidative stress independently of Aβ accumulation [36] suggesting that the neurovascular alterations observed in this model are in part the result of oxidative stress induced by Aβ accumulation. Furthermore, cerebral hypoperfusion has been shown to lead to the accumulation of amyloid in the brain [20]. Together, this evidence suggested a possible mechanism by which chronic cerebral hypoperfusion may lead to progression of dementia by promoting degenerative changes, such as microinfarcts, and increased Aβ deposition through oxidative stress pathways. However the evidence linking these pathways was lacking.

This study aimed to build on our previous work to investigate the long-term effects of mild cerebral hypoperfusion in TgAPP mice with the prediction that this would lead to alterations in Aβ pools causing vascular amyloid accumulation and degenerative changes, the latter of which would be more severe than in wild-type mice lacking Aβ. The effects of mild chronic

cerebral hypoperfusion on the dynamics of Aβ 40/42 pools were assessed in the parenchyma and vasculature of TgAPP mice. Since both hypoperfusion and Aβ have been linked to the presence of microinfarcts, the load of these and haemorrhagic lesions were measured. Furthermore, potential links between hypoperfusion, Aβ and NOX2 with the development of microinfarcts were investigated.

Methods

Animals

Transgenic mice (Tg-SwDI) overexpressing the human APP, harbouring the Swedish K670N/M671L, Dutch E693Q and Iowa D694N mutations under the control of the Thy1 promoter [37] on a C57Bl/6J background were purchased from Jackson Laboratories and subsequently bred in house and maintained on a homozygous background. Wild type mice (C57Bl/6J) were purchased from Charles River Laboratories. All procedures were authorized under the project licence number 60/4350 held by Prof. Horsburgh, approved by the UK Home Office and the University of Edinburgh's Ethical Review Committee and adhered to regulations specified in the Animals (Scientific Procedures) Act (1986).

Chronic cerebral hypoperfusion

Chronic cerebral hypoperfusion was induced as previously described in mice at 4-5months old [6-10]. Mice were anaesthetized with 1.5% isoflurane, and microcoils (0.18 mm internal diameter; Sawane Spring Co. Japan) were applied permanently to both common carotid arteries. Sham animals underwent identical surgical interventions without application of microcoils. The recovery of the mice was closely monitored with weight and general health

recorded regularly. The surgeon was blind to the genotype of the mice and the final analysis were conducted blind to the surgical intervention and genotype.

Tissue processing for histopathology

At either 1 month (Tg-SwDI: n = 9 sham/10 hypoperfused; wild-type: n = 12 sham/11 hypoperfused) or 3 months (Tg-SwDI: n = 9 sham/ 9 hypoperfused; wild-type: n = 10 sham/10 hypoperfused) after surgery, mice were transcardially perfused with 20 ml of heparinized phosphate buffered saline (PBS) and then with 20 ml of 4% paraformaldehyde (PFA) in 0.1% phosphate buffer (pH 7.4). After perfusion brains were removed, cut along the midline and both hemibrains were post-fixed in 4% PFA for 24 hours. The left hemibrain was washed for 1 hour in phosphate buffer and 30 μm thick sagittal sections were produced with a vibratome (Hydrax V50, Zeiss). Sections were collected and stored in cryoprotective medium (30% glycerol/30% ethylene glycol/40% PB) at -20ºC until use. The right hemibrain was transferred to 70% ethanol followed by paraffin processing and sagittal sections (6 μm thickness) were cut for quantification of microinfarcts and haemorrhages.

Immunohistochemistry

Immunohistochemistry was carried out according to standard procedures. Vibratome sections, at anatomical level corresponding to 1.92 mm from midline were rinsed with PBS followed by tris-buffer (pH 7.6) and then mounted onto superfrost plus slides (VWR International). Sections were incubated through a series of alcohols (100%, 90% and 70% ethanol) and then equilibrated in PBS 0.1% triton. Antigen retrieval was performed by submerging slices in 10 mM citrate buffer (pH 6) at 100 °C under pressure for 10 minutes. Subsequently, retrieval using 10% proteinase K for 10 minutes at room temperature was performed. Samples were blocked with 20% normal serum 0.5% BSA and then incubated

with the antibody solution (6E10 1:1000, Sigma 39320; anti-collagen IV 1:800, Fitzgerald 70R-CR013x), overnight at 4 °C. Finally, antigens were visualized by incubating with the secondary antibody solution (anti-rabbit alexa fluor 546 1:500, Invitrogen A11010; anti-mouse alexa fluor 488 1:500, Invitrogen A11001).

Paraffinized tissue slices, at anatomical levels corresponding to 1.56 mm and 1.92 mm from midline were deparaffinized with heat (60 °C) followed by incubation in xylene. Samples were later incubated in 100% ethanol and then covered with 3% H_2O_2. Citrate retrieval was performed as described above. Subsequently, tissue sections were blocked with 10% serum 0.5% BSA and then incubated with anti-Iba1 1:1000 (Menarini MP290) overnight at 4 °C. Slides were incubated with biotinylated anti-rabbit 1:100 (Vector BA1000) for 1 hour at room temperature followed by incubation with Vectastain Elite ABC reagent (Vector Labs). Antigens were visualized with diaminobenzidine solution (Vector Labs).

Analysis of immunohistochemistry

Immunolabelled vibratome sections were analysed using a laser scanning confocal microscope (Zeiss LSM 510, Germany). Images were selected from the thalamus since this is a brain region in TgSwDI mice that has most amyloid deposition with age. Four images of the thalamus per brain were acquired with a 40x objective at a 1024 x 1024 pixel resolution. Parenchymal Aβ load was determined by subtracting the percentage of vascular staining within a defined area from the percentage of Aβ staining in that area. Colocalization analysis for blood vessels and Aβ was done by calculating the Manders coefficient and data presented as % vascular amyloid. Images from immunolabelled paraffin sections were acquired at 4x magnification using a QImaging QICAM MicroPulisher 3.3 camera (QImaging, Surrey, BC, Canada) connected to a Olympus BX51 microscope (Olympus UK, Southendon-Sea, UK).

Microglial burden was assessed by measuring the percentage of stained area occupied by Iba1 immunostaining. All measurements were carried out using Image J software (v1.42q).

Histological detection of microinfarcts and haemorrhages

Deparaffinized sections were stained with haematoxylin and eosin (H&E) and Perls Prussian blue using standard protocols to determine the presence of ischaemic tissue damage and haemorrhages respectively. Tissue sections at anatomical level corresponding to -1.70 and -2.18 mm from Bregma were analysed and two sections per mouse. Four images of the thalamus were acquired at 10x magnification. Microinfarcts were defined as sharply delineated areas of tissue pallor on H&E sections that were accompanied by microglial proliferation identified by Iba1 immunostaining in adjacent sections. The area covered by infarcted tissue was measured using Image J software (v1.42q). Haemorrhages were identified by the presence of ferric iron deposits on Perls stained sections (Supplementary Fig. S1, b). The presence or absence of haemorrhages in each mouse was recorded.

Generation of parenchymal and vessel enriched fractions

At either 1 month (n = 10 sham/9 hypoperfused) or 3 months (n = 6/sham/ 6 hypoperfused group) after surgery, mice were transcardially perfused under 5% isoflurane anaesthesia with 20 ml 0.9% heparinized PBS (pH 7.4). The brains were removed and cut along the midline. The left hemibrain was homogenized with a fit dounce homogenizer with 1 ml of PBS on ice, using 15 strokes. The homogenate was centrifuged at 250 x g for 10 minutes at 4^0C. The pellet was re-suspended in 3 ml of 17.5% ficoll (Sigma) and centrifuged at 3,200 x g for 25 minutes. The pellet (containing the vessel enriched fraction) was collected and the supernatant (containing the parenchymal fraction) was centrifuged again at 3,200 x g for 25 minutes. The pellets from both spins were re-suspended in 1 ml of 1% BSA-PBS and

centrifuged at 2,000 x g for10 minutes. The pellet was washed with 1 ml of PBS and stored at -80^{0}C. The supernatant containing the parenchymal fraction was mixed with 6 ml of PBS and centrifuged at 3,200 x g for10 minutes. The supernatant was discarded and the pellet stored at -80^{0}C.

Protein extraction and quantification

Sequential protein extraction was performed in order to obtain both soluble and insoluble protein fractions. Briefly, the tissue was homogenized with homogenization buffer (20 mM tris base pH 7.4, 250 mM sucrose, 1 mM EDTA, 1 mM EGTA, 1X protease inhibitor cocktail [Calbiochem]) and centrifuged at 100,000 x g for 1 hour at 4^{0}C. The supernatant (containing the soluble protein fraction) was carefully transferred to a new tube and stored at -80^{0}C. The pellet was resuspended and homogenized in guanidine buffer (5 M guanidine, 50 mM Tris/HCL) and mixed for 3 hours at room temperature (RT). The solution was diluted 1:10 with ice-cold reaction buffer (0.2 g/L KCL, 0.2 g/L KH2PO4, 8 g/L NaCl, 1.15 g/L Na2HPO4, 5% BSA, 0.03% Tween 20, 1X protease inhibitor cocktail) and centrifuged at 16,000 x g for 20 minutes at 4^{0}C. The supernatant (containing the insoluble protein fraction) was stored at -80^{0}C. Total protein extraction was performed by re-suspending the tissue in RIPA buffer (50 mM Tris, pH 7.5, 1% NP-40, 150 mM NaCl, 1 mM EDTA, 0.1% SDS, 0.5% sodium deoxycholate, 1X protease inhibitor cocktail), followed by sonication for 5 seconds at 10% amplitude (Branson digital sonifier) Samples were centrifuged at 5000 x g. for 5 minutes and the supernatant was collected and stored at -80^{0}C. Protein levels were quantified with Pierce BCA Protein Assay Kit (Thermo Scientific).

Enzyme-linked immunosorbent assay (ELISA)

Levels of both Aβ1-40 and Aβ1-42 were determined by ELISA (Invitrogen) in the soluble and insoluble protein fractions extracted from the parenchymal and the vessel enriched fractions. NOX2 levels were assessed by ELISA (Cusabio) in total proteins extracted from brain homogenates. In all experiments, manufacturer's instructions were used to perform the assays.

Western blot

Total proteins extracted from brain homogenates were used to detect full-length APP and APP-carboxyl terminal fragments (CTF's). Proteins were fractionated by electrophoresis using 4–12% sodium dodecyl sulphate polyacrylamide gels (Invitrogen), electroblotted into PVDF membranes (Hybond-P, GE Healthcare) and incubated with the different antibodies (anti-APP, MAB348, anti-APP-CTF, Calbiochem 171610,). The immunoreactive bands were visualized using the Odyssey Infrared Imaging System (LiCor Biosciences, Lincoln, NE, USA).

Statistical analysis

The % parenchymal and vascular Aβ measurements (confocal imaging) were analysed for statistical significance between groups using Mann-Whitney U statistic with $p < 0.05$. ELISA and western blot analyses were analysed for statistical significance between groups using unpaired t-test with $p < 0.05$. For NOX2 ELISA and microinfarct studies, statistical comparison was carried out using two-way analysis of variance (with genotype and surgery as the factors) and, if data were significant ($p<0.05$), followed by the Bonferroni post-test. The number of haemorrhages were analysed for statistical significance between groups using

Fishers exact test. For association analyses, Pearson correlation coefficient was used. All analyses were performed using Graph Pad Prism 5.0 software (La Jolla, CA, USA).

Results

Soluble Aβ levels are increased in response to cerebral hypoperfusion and precede insoluble Aβ accumulation in the parenchyma

Initial experiments were undertaken to examine the effect of cerebral hypoperfusion on the levels and pools (soluble and insoluble) of Aβ. These experiments were undertaken in Tg-SwDI mice and not wild-type mice. Aβ is quite different in wild-type rodents as compared to transgenic mice with human APP mutations. In particular wild-type rodents do not naturally accumulate fibrillar Aβ with age most likely due to differences in the amino acid structure of Aβ [38]. Tg-SwDI mice develop Aβ deposits with increasing age and thus Aβ dynamics can be readily studied in this line [37]. In this study Tg-SwDI mice were analysed at an age when parenchymal Aβ deposition (and vascular) is moderate and predominantly diffuse in nature to assess the vulnerability to disease progression in the presence of hypoperfusion. There was no discernable effect of cerebral hypoperfusion on the cellular localization of Aβ (Fig. 1). Quantification of the parenchymal load of the protein (% parenchymal Aβ) indicated that this was not significantly different between sham and hypoperfused Tg-SwDI mice after either 1 or 3 months ($p>0.05$). To further investigate whether chronic hypoperfusion may have an effect on the different pools of Aβ within the parenchyma, the levels of soluble and insoluble Aβ were quantified by ELISA. After 1 month of hypoperfusion, significantly increased levels

of both Aβ40 (p=0.02) and Aβ42 (p=0.02) were found in the soluble protein fraction, when compared to the sham control. In contrast, the insoluble protein fraction remained unchanged (p>0.05). After 3 months of hypoperfusion, there were no significant changes between the sham and hypoperfused groups in the soluble fraction (p>0.05), however increased concentrations of both Aβ40 (p=0.002) and Aβ42 (p=0.008) were observed in the insoluble fraction (Fig. 2). These data suggest that hypoperfusion can modify Aβ metabolism, triggering an early increase of soluble Aβ protein followed by aggregation into insoluble fibrils in the parenchyma.

Delayed accumulation of vascular Aβ in response to cerebral hypoperfusion

Tg-SwDI mice have a well characterized vascular accumulation of Aβ starting from 3 months of age particularly in the thalamus. To determine if cerebral hypoperfusion may exacerbate vascular accumulation of Aβ in these mice, confocal microscopy was used to quantify Aβ colocalization within the vasculature. After 1 month of hypoperfusion there were no changes in the levels of Aβ colocalized to vessels between sham and hypoperfused mice (p > 0.05, Fig. 3a). Conversely, following 3 months of hypoperfusion, the levels of Aβ colocalized to vessels significantly increased in the hypoperfused animals (p=0.04), compared to the sham group (Fig. 3b-d, see arrows). To further examine the pools of Aβ, the levels of Aβ40/42 were measured in protein extracts from vessel enriched fractions (Fig. 4). There were no significant changes in the levels of soluble/insoluble Aβ40/42 determined between hypoperfused and sham animals after 1 month of hypoperfusion (p>0.05). However, following 3 months there was a significant increase in the levels of both Aβ40 (p=0.002) and Aβ42 (p=0.008) in the insoluble fraction of the hypoperfused group when compared to the shams and notably soluble levels of Aβ40/42 were unchanged (p>0.05). Collectively, these

results indicate that hypoperfusion promotes the build-up of fibrillar Aβ in the cerebrovasculature, a process that is preceded by an increase in soluble Aβ.

Chronic cerebral hypoperfusion increases APP levels and processing

To investigate the mechanisms by which cerebral hypoperfusion may lead to increased Aβ levels we next sought to determine whether this process was mediated by increased amyloid precursor protein (APP) production or processing. Western blot analysis of brain protein extracts was performed using specific antibodies that recognise full-length APP and its C-terminal fragments (CTF's), produced after proteolytic cleavage of APP by the specific enzymes; β-secretase that generates CTFβ and α-secretase that results in the formation of CTFα (Fig. 5). Interestingly, the immunoblotting analysis revealed a significant increase in the levels of APP ($p=0.0008$), CTFβ ($p=0.0002$) and CTFα ($p<0.0001$) in the hypoperfused animals following 1 month, when compared to the sham group, (Fig. 5a, c-e); however, after 3 months of hypoperfusion no difference was observed between the two groups ($p>0.05$, Fig. 5b, f-h), suggesting that the increased Aβ levels observed, might be the result of enhanced APP synthesis and processing, triggered at early stages during chronic cerebral hypoperfusion.

Microinfarcts and microhemorrhages are precipitated by chronic cerebral hypoperfusion and Aβ

The effect of chronic cerebral hypoperfusion and potential interaction with amyloid on the development of microinfarcts was examined in wild-type and Tg-SwDI mice following 1 and

3 months hypoperfusion compared to shams (Fig. 6). Microinfarcts were identified in H&E sections as areas of tissue pallor and in adjacent sections stained with Iba1 to identify microglial proliferation (Fig. 6a-d). There was no evidence of microinfarcts in sham wild-type mice but small areas of infarcted tissue were observed in sham Tg-SwDI animals (Fig. 6e,f). After cerebral hypoperfusion there was a marked increase in microinfarcts that was exacerbated in Tg-SwDI mice. At one month there was a significant effect of genotype ($F_{(1,38)} = 14.52$, $p = 0.0005$) and an increase in infarct area in TgSwDI mice was determined. The area of infarct was significantly greater in hypoperfused TgSwDI mice compared to sham TgSwDI mice ($p < 0.05$). At three months following hypoperfusion there was a significant effect of surgery ($F_{(1,34)} = 10.1$, $p = 0.003$) and genotype ($F_{(1,34)} = 21.8$, $p < 0.0001$), and furthermore there was a significant interaction ($F_{(1,34)} = 5.45$, $p = 0.03$) between surgery and genotype with a greater volume of infarct in hypoperfused TgSwDI mice ($p < 0.01$). Together, this data indicates that chronic cerebral hypoperfusion increases microinfarct burden and that this is exacerbated in Tg-SwDI mice.

There was no evidence of haemorrhages in any sham wild-type or TgSwDI mice and following 1 month of hypoperfusion in wild-type or TgSwDI mice. However after 3 months of hypoperfusion, haemorrhages were evident in one wild-type mouse and three Tg-SwDI mice in subcortical thalamic regions albeit this was not statistically significant (Supplementary Fig. S1).

Aβ increases NOX2 levels, which is exacerbated by chronic cerebral hypoperfusion

In order to examine the effect of both Aβ and chronic cerebral hypoperfusion on oxidative stress, quantitative ELISA measurement of brain protein extracts were assayed to determine

the levels of NADPH oxidase 2 (NOX2), the main reactive oxygen species (ROS) generator in the brain (Fig. 7). At one month, there was a significant effect of surgery ($F_{(1,29)} = 4.29$, $p = 0.047$) and significant effect of genotype ($F_{(1,29)} = 16.8$, $p = 0.0003$) on NOX2 levels but there was no significant interaction. Follow up post-hoc analysis indicated that NOX2 levels were significantly increased in Tg-SwDI hypoperfused mice compared to Tg-SwDI shams ($p<0.05$) but there was no difference between wild-type sham and hypoperfused mice (Fig. 7a). At 3 months, there was no significant effect of surgery ($p<0.05$) but there was a significant effect of genotype ($F_{(1,23)} = 4.7$, $p = 0.04$) (Fig. 7b) with no significant interaction ($p > 0.05$). Thus NOX2 levels were elevated in Tg-SwDI mice. Interestingly, the increased levels of NOX2 positively correlated with the levels of soluble parenchymal Aβ ($r = 0.66$, $p = 0.002$) (Fig. 7c**)** but no correlation was observed with levels of cerebrovascular Aβ ($r = 0.085$, $p = 0.73$) (Fig. 7d).

Discussion

Considerable evidence indicates that cerebral hypoperfusion, an early feature of AD brains, is implicated in degenerative processes and cognitive decline [1-5]. The present study sought to probe potential mechanistic links and investigated the effects of chronic cerebral hypoperfusion on Aβ dynamics in the brain of Tg-SwDI mice and its relationship with the development of microinfarcts. We demonstrated that mild cerebral hypoperfusion modifies Aβ metabolism, triggering an early increase in the levels of soluble Aβ in the parenchyma followed by aggregation of the protein into insoluble fibrils, with the subsequent build-up of aggregates in the cerebrovasculature. Furthermore, our study showed that the extent of microinfarcts associated with microglial proliferation was increased with hypoperfusion and

exacerbated in the Tg-SwDI mice. Soluble parenchymal Aβ levels in Tg-SwDI mice were associated with elevated NOX2.

Previous studies have provided conflicting evidence that modest reductions in cerebral perfusion can induce enhancement [20,39,40] and suppression [41] of Aβ deposition. In the present study, we show that soluble Aβ levels are increased in response to mild cerebral hypoperfusion at one month and precede insoluble Aβ accumulation in the parenchyma at 3months. We suggest that the amount of parenchymal Aβ produced exceeds the capacity of normal clearance mechanisms, and thus Aβ proceeds to accumulate in the vessel walls, at the clearance site. Thereafter, new Aβ molecules synthesized will likely adhere to the growing fibrils in the parenchyma and vasculature. Our results support previous studies showing that cerebral amyloid angiopathy (CAA) is preceded by higher levels of soluble amyloid suggesting that soluble Aβ is a marker of potential CAA [42,43].

Increased parenchymal Aβ levels, in response to hypoperfusion, might be the result of either overproduction or altered clearance of the protein, or the combination of both. Here, we show enhanced APP synthesis and processing, triggered at early stages during chronic cerebral hypoperfusion, which suggests that the increased Aβ levels observed might be the result of a general increase in APP metabolism, where both amyloidogenic and non-amyloidogenic pathways are enhanced. The latter can be concluded by the observation of increased levels of both C-terminal fragments (CTFs), CTFβ and CTFα respectively. Although the physiological function of APP is not completely understood, there is well documented evidence of a neurotrophic and synaptogenic role of the full-length protein [44-46]. Moreover, there are a number of studies showing that ischaemic injury induces intra-axonal upregulation of APP or increases its processing to smaller fragments [46, 47]. Thus initially, upregulation of APP and

increased metabolism in response to hypoperfusion might be directly linked to its neuroprotective role. Notably though these effects on APP were short-lived and absent at 3months post-hypoperfusion at which time an increase in insoluble Aβ was detected.

Clearance of cerebral Aβ is complex and regulated by several different processes including transport across the blood brain barrier (BBB) [48], engulfment and degradation by microglia/macrophage [48] and drainage pathways [48-50]. Our work has shown that BBB changes are not evident until six months after hypoperfusion [10] and would suggest that this is not a key mechanism leading to amyloid accumulation. Further the levels of low density lipoprotein receptor-related protein (LRP) and receptor for advanced glycation endproducts (RAGE), important in trafficking Aβ across the BBB, are not altered with hypoperfusion (data not shown). Increased microglia were evident in the present study but it is not yet known whether alterations in microglia function or phagocytosis may contribute to the accumulation of Aβ. In a previous study of severe chronic cerebral hypoperfusion microglial dysfunction and decreased phagocytic activity was suggested to contribute to enhanced Aβ deposition [51]. There is growing evidence that drainage pathways also play a vital role in the clearance of Aβ and are impacted by CAA. Thus these potential mechanisms leading to Aβ accumulation should be explored in the hypoperfusion model.

Cerebral microinfarcts constitute a common observation in AD brains [12,13] and, as shown by several studies, the load of these infarcts correlates with impaired cognitive performance [52-54]. In this study, we show that the development of microinfarcts associated with microglial proliferation, is precipitated by chronic cerebral hypoperfusion, suggesting a link between hypoperfusion and the development of vascular lesions. Additionally, vascular accumulation of Aβ, which is present in almost all cases of AD, has been linked with the

development of microinfarcts. However, the analysis of the association between CAA and microinfarct load remains inconclusive, with data showing a positive correlation [17,18] or no correlation [55] between these measures. To further examine the link between microinfarct load and Aβ deposition, we performed association analyses, which surprisingly revealed no correlation between microinfarct load and vascular or parenchymal amyloid levels (data not shown). However, notably the appearance of microinfarcts was exacerbated in the hypoperfused Tg-SwDI mice compared to wild-types, suggesting an underlying influence of amyloid on the development of these lesions. One explanation to this result might be attributable to the fact that the association analyses were conducted using the quantification of the amyloid immunostaining which does not distinguish between the different pools of Aβ. Therefore, we hypothesize that rather than insoluble aggregates, soluble Aβ oligomers, which constitute the most cytotoxic species of Aβ, might be involved on the development of microinfarcts (see Fig. 8). Differences in Aβ pools could also explain the inconsistencies in findings between the previous studies. Indeed, compelling evidence supports the oligomer hypothesis, which suggests that soluble Aβ oligomers are the main etiologic agent that participates in the initiation of the neurodegenerative process in AD, by triggering a cascade of pathogenic events involving inflammation and oxidative injury [56-60].

Previous studies have shown a significant association between oxidative stress and the development of microinfarcts [23-28]. Consequently, to further investigate the potential mechanistic basis of our current finding of increased microinfarction following chronic cerebral hypoperfusion, we studied the levels of NOX2. We found higher NOX2 levels in the Tg-SwDI mice compared to the wild-type controls, and this was exacerbated by hypoperfusion (at one month) in the transgenic model, suggesting an additive effect, where

both amyloid and hypoperfusion contribute to NOX2 upregulation. Thus, NOX2-derived radicals may have contributed to the development of microinfarcts. Interestingly, in agreement with our previous hypothesis, rather than vascular Aβ, soluble parenchymal Aβ correlated with increased NOX2 levels, suggesting the potential participation of these species in the pathoetiology of microinfarcts.

The evidence from the present study points towards a mechanism by which chronic cerebral hypoperfusion leads to an imbalance in the dynamics of Aβ metabolism. We propose a mechanistic pathway for the contribution of chronic cerebral hypoperfusion to cognitive decline and mechanisms relevant to AD (Fig. 8). Chronic cerebral hypoperfusion may initially increase the generation of soluble Aβ or Aβ oligomers that promote pro-inflammatory and oxidative stress mechanisms (such as NOX2) leading to degenerative changes such as microinfarcts. Over time Aβ may accumulate, particularly in the vasculature, exacerbating vascular dysfunction and accelerating degenerative changes and cognitive decline thus promoting a vicious cycle of events. In previous studies, cerebral hypoperfusion has been shown to impact spatial working memory in wild-type mice [6,10]. It would be of translational value to determine whether cerebral hypoperfusion in TgAPP mice exacerbates the cognitive impairment and to further define mechanistically the interactions between hypoperfusion and Aβ.

Acknowledgements:

NS was supported by a studentship from AXA foundation. The research was further supported by grants from the Alzheimer Society (152 (PG-157)), Alzheimer Research UK (ART-PG2010-3; ARUK-PG2013-22), and The University of Edinburgh Centre for Cognitive Ageing and Cognitive Epidemiology, part of the cross council Lifelong Health and Wellbeing Initiative (G0700704/84698).

References:

1. Kalaria, R.N., and Ince, P. (2000) Vascular factors in Alzheimer's disease. *Ann N Y Acad Sci*. **903**, 1–552.
2. Iturria-Medina, Y., Sotero, R.C., Toussaint, P.J., Mateos-Pérez, J.M., and Evans, A.C.; Alzheimer's Disease Neuroimaging Initiative. (2016) Early role of vascular dysregulation on late-onset Alzheimer's disease based on multifactorial data-driven analysis. *Nat Commun*. **21**,7:11934.
3. Ruitenberg, A., den Heijer, T., Bakker, S.L., van Swieten, J.C., Koudstaal, P.J., Hofman, A., and Breteler, M.M. (2005) Cerebral hypoperfusion and clinical onset of dementia: the Rotterdam Study. *Ann Neurol*. **57**, 789-794.
4. Alsop, D.C., Dai, W., Grossman, M., and Detre, J.A. (2010) Arterial spin labeling blood flow MRI: it's role in the early characterization of Alzheimer's disease. *J Alzheimers Dis*. **20(3),** 871-80.
5. Chao, L.L., Buckley, S.T., Kornak, J., Schuff, N., Madison, C., Yaffe, K., Miller, B.L., Kramer J.H., and Weiner M.W. (2010) ASL perfusion MRI predicts cognitive decline and conversion from MCI to dementia. *Alzheimer Dis Assoc Disord*. **24(1)**, 19-27.
6. Coltman, R., Spain, A., Tsenkina, Y., Fowler, J.H., Smith, J., Allerhand, M., Scott, F., Kalaria, R.N., Ihara, M., Daumas, S., Deary, I.J., Wood, E., McCulloch, J., and Horsburgh, K. (2011) Spatial memory in mice remains intact despite widespread white matter pathology *Neurobiol Aging* **32(12)**, 2324.e7-2324.e12.
7. Holland, P.R., Bastin, M.E.., Jansen, M.A., Merrifield, G.D., Coltman, R.B., Scott, F., Nowers, H., Khallout, K., Marshall, I., Wardlaw, J., Deary, I.J., McCulloch, J., and Horsburgh, K. (2011) MRI is a sensitive marker of subtle white matter pathology in hypoperfused mice. *Neurobiol Aging* **32(12)**, 2325.e1-6.
8. Reimer, M.M., McQueen, J., Searcy J.L., Zonta, B., Desmazieres, A., Smith, J., Gliddon, C., Scullion, G., Wood, E., Herzyk, P., Brophy, P., McCulloch, J., and Horsburgh, K. (2011) Rapid disruption of axon-glial integrity in response to mild cerebral hypoperfusion. *J Neurosci* **31(49)**, 18185-94.
9. McQueen, J., Reimer, M.M., Holland, P.R,, and Horsburgh, K. (2014) Restoration of oligodendrocyte pools in a mouse model of chronic cerebral hypoperfusion *Plos One* **9(2)**, e87227.
10. Holland, P.R., Searcy, J.L., Salvadores, N., Scullion, G., Chen, G., Lawson, G., Scott, F., Bastin, M.E., Ihara, M., Kalaria, R.N., Wood, E.R., Smith, C., Wardlaw, J.M., and Horsburgh, K. (2015) Gliovascular disruption and cognitive deficits in a mouse model with features of small vessel disease. *J Cereb Blood Flow Metab*. **35(6)**, 1005-14
11. Shibata, M., Ohtani, R., Ihara, M., and Tomimoto, H. (2004). White matter lesions and glial activation in a novel mouse model of chronic cerebral hypoperfusion. *Stroke* **35(11)**, 2598-2603.
12. Brundel, M., de Bresser, J., van Dillen, J.J., Kappelle, L.J. and Biessels, G.J. (2012) Cerebral microinfarcts: a systematic review of neuropathological studies. *J Cereb Blood Flow Metab*. **32**, 425-436.
13. van Rooden, S., Goos, J.D., van Opstal, A.M., Versluis, M.J., Webb, A.G., Blauw, G.J., van der Flier, W.M., Scheltens, P., Barkhof, F., van Buchem, M.A., and van der Grond, J.(2014) Increased number of microinfarcts in Alzheimer disease at 7-T MR imaging. *Radiology*. **270**, 205-211.

14. Olichney, J.M., Hansen, L.A., Hofstetter, C.R., Grundman, M., Katzman, R., and Thal, L.J. (1995) Cerebral infarction in Alzheimer's disease is associated with severe amyloid angiopathy and hypertension. *Arch Neurol*. **52**, 702-708.
15. Haglund, M., Sjöbeck, M. and Englund, E. (2004) Severe cerebral amyloid angiopathy characterizes an underestimated variant of vascular dementia. *Dement Geriatr Cogn Disord*. **18**, 132-137.
16. Haglund, M., Passant, U., Sjöbeck, M., Ghebremedhin, E., and Englund, E. (2006) Cerebral amyloid angiopathy and cortical microinfarcts as putative substrates of vascular dementia. *Int J Geriatr Psychiatry*. **21**, 681-687.
17. Okamoto, Y,, Ihara, M., Fujita, Y., Ito, H., Takahashi, R., and Tomimoto, H. (2009) Cortical microinfarcts in Alzheimer's disease and subcortical vascular dementia. *Neuroreport*. **20**, 990-996.
18. Soontornniyomkij, V., Lynch, M.D., Mermash, S., Pomakian, J., Badkoobehi, H., Clare, R., and Vinters, H.V. (2010) Cerebral microinfarcts associated with severe cerebral beta-amyloid angiopathy. *Brain Pathol*. **20**, 459-467.
19. Suter, O.C., Sunthorn, T., Kraftsik, R., Straubel, J., Darekar, P., Khalili, K., and Miklossy, J. (2002) Cerebral hypoperfusion generates cortical watershed microinfarcts in Alzheimer disease. *Stroke*. **33**, 1986-1992.
20. Okamoto, Y., Yamamoto, T., Kalaria, R.N., Senzaki, H., Maki, T., Hase, Y., Kitamura, A., Washida, K., Yamada, M., Ito, H., Tomimoto, H., Takahashi, R., and Ihara, M. (2012) Cerebral hypoperfusion accelerates cerebral amyloid angiopathy and promotes cortical microinfarcts. *Acta Neuropathol*. **123**, 381-194.
21. Smith, E.E., Schneider, J.A., Wardlaw, J.M. and Greenberg, S.M. (2012) Cerebral microinfarcts: the invisible lesions. *Lancet Neurol*. **11**, 272-282.
22. Miklossy, J. (2003) Cerebral hypoperfusion induces cortical watershed microinfarcts which may further aggravate cognitive decline in Alzheimer's disease. *Neurol Res*. **25**, 605-610.
23. Damasceno, B.P. (2012) Relationship between cortical microinfarcts and cognitive impairment in Alzheimer's disease. *Dement Neuropsychol*. **6**, 131-136.
24. Chen, H., Kim, G.S., Okami, N., Narasimhan, P. and Chan, P.H. (2011) NADPH oxidase is involved in post-ischemic brain inflammation. *Neurobiol Dis*. **42**, 341-348.
25. Brennan-Minnella, A.M., Won, S.J. and Swanson, R.A. (2014) NADPH Oxidase-2: Linking Glucose, Acidosis, and Excitotoxicity in Stroke. *Antioxid Redox Signal*. **22**, 161-174.
26. Walder, C.E., Green, S.P., Darbonne, W.C., Mathias, J., Rae, J., Dinauer, M.C., Curnutte, J.T., and Thomas, G.R. (1997) Ischemic stroke injury is reduced in mice lacking a functional NADPH oxidase. *Stroke*. **28**, 2252-2258.
27. Tang, X.N., Cairns, B., Cairns, N., and Yenari, M.A. (2008) Apocynin improves outcome in experimental stroke with a narrow dose range. *Neuroscience*. **154**, 556-162.
28. Jackman, K.A., Miller, A.A., De Silva, T.M., Crack, P.J., Drummond, G.R., and Sobey, C.G. (2009) Reduction of cerebral infarct volume by apocynin requires pretreatment and is absent in Nox2-deficient mice. *Br J Pharmacol*. **156**, 680-688.
29. Bianca, V.D., Dusi, S., Bianchini, E., Dal Prà, I., and Rossi F. (1999) beta-amyloid activates the O-2 forming NADPH oxidase in microglia, monocytes, and neutrophils. A possible inflammatory mechanism of neuronal damage in Alzheimer's disease. *J Biol Chem*. **274**, 15493-15499.
30. Coraci, I.S., Husemann, J., Berman, J.W., Hulette, C., Dufour, J.H., Campanella, G.K, Luster, A.D., Silverstein, S.C., and El-Khoury, J.B. (2002) CD36, a class B scavenger receptor, is expressed on microglia in Alzheimer's disease brains and can mediate

production of reactive oxygen species in response to beta-amyloid fibrils. *Am J Pathol*. **160**, 101-112.
31. Abramov, A.Y., Canevari, L., and Duchen, M.R. (2004) Beta-amyloid peptides induce mitochondrial dysfunction and oxidative stress in astrocytes and death of neurons through activation of NADPH oxidase. *J Neurosci*. **24**, 565-575.
32. Qin, B., Cartier, L., Dubois-Dauphin, M., Li, B., Serrander, L., and Krause, K.H. (2006) A key role for the microglial NADPH oxidase in APP-dependent killing of neurons. *Neurobiol Aging*. **27**, 1577-1587.
33. Wilkinson, B.L. and Landreth, G.E. (2006) The microglial NADPH oxidase complex as a source of oxidative stress in Alzheimer's disease. *J Neuroinflammation*. **3**, 30
34. Narayan, P., Holmström, K.M., Kim, D.H., Whitcomb, D.J., Wilson, M.R., St George-Hyslop, P., Wood, N.W., Dobson, C.M., Cho, K., Abramov, A.Y., and Klenerman, D. (2014) Rare individual amyloid-β oligomers act on astrocytes to initiate neuronal damage. *Biochemistry*. **53**, 2442-2453.
35. Parajuli, B., Sonobe, Y., Horiuchi, H., Takeuchi, H., Mizuno, T., and Suzumura, A. (2013) Oligomeric amyloid β induces IL-1β processing via production of ROS: implication in Alzheimer's disease. *Cell Death Dis*. **4**, e975.
36. Park, L., Zhou, P., Pitstick, R., Capone, C., Anrather, J., Norris, E.H., Younkin, L., Younkin, S., Carlson, G., McEwen, B.S., and Iadecola, C. (2008) Nox2 derived radicals contribute to neurovascular and behavioral dysfunction in mice overexpressing the amyloid precursor protein. *Proc Natl Acad Sci U S A.* **105**, 1347-1352.
37. Davis, J., Xu, F., Deane, R., Romanov, G., Previti, M.L., Zeigler, K., Zlokovic, B.V., and Van Nostrand, W.E. *(*2004) Early-onset and robust cerebral microvascular accumulation of amyloid beta-protein in transgenic mice expressing low levels of a vasculotropic Dutch/Iowa mutant form of amyloid beta-protein precursor. *J Biol Chem*. **279**, 20296-20306 (2004).
38. Dyrks, T., Dyrks, E., Masters, C.L., and Beyreuther, K. (1993) Amyloidogenicity of rodent and human beta A4 sequences. *FEBS Lett*. **324**:231–6.
39. Kitaguchi, H., Tomimoto, H., Ihara, M., Shibata, M., Uemura, K., Kalaria, R.N., Kihara, T., Asada-Utsugi, M., Kinoshita, A., and Takahashi, R. (2009) Chronic cerebral hypoperfusion accelerates amyloid beta deposition in APPSwInd transgenic mice. *Brain Res*. **1294**, 202-210.
40. Elali, A., Thériault, P., Préfontaine, P. and Rivest, S. (2013) Mild chronic cerebral hypoperfusion induces neurovascular dysfunction, triggering peripheral beta-amyloid brain entry and aggregation. *Acta Neuropathol Commun*. **1**, 75 (2013).
41. Yamada, M., Ihara, M., Okamoto, Y., Maki, T., Washida, K., Kitamura, A., Hase, Y., Ito, H., Takao, K., Miyakawa, T., Kalaria, R.N., Tomimoto, H., and Takahashi, R. (2011) The influence of chronic cerebral hypoperfusion on cognitive function and amyloid β metabolism in APP overexpressing mice. *PLoS One*. **6**, e16567 .
42. Suzuki, N., Iwatsubo, T., Odaka, A., Ishibashi, Y., Kitada, C., and Ihara, Y. (1994) High tissue content of soluble beta 1-40 is linked to cerebral amyloid angiopathy. *Am J Pathol*. **145**, 452-460.
43. Shinkai, Y., Yoshimura, M., Ito, Y., Odaka, A., Suzuki, N., Yanagisawa, K., and Ihara, Y. (1995) Amyloid beta-proteins 1-40 and 1-42(43) in the soluble fraction of extra- and intracranial blood vessels. *Ann Neurol*. **38**, 421-428.
44. Caillé, I., Allinquant, B., Dupont, E., Bouillot, C., Langer, A., Müller, U., and Prochiantz, A. (2004) Soluble form of amyloid precursor protein regulates proliferation of progenitors in the adult subventricular zone. *Development*. **131**, 2173-2181.

45. Stephenson, D.T., Rash, K. and Clemens, J.A. (1992) Amyloid precursor protein accumulates in regions of neurodegeneration following focal cerebral ischemia in the rat. *Brain Res.* **593**, 128-135.
46. Bennett, S.A., Pappas, B.A., Stevens, W.D., Davidson, C.M., Fortin, T. and Chen, J. (2000) Cleavage of amyloid precursor protein elicited by chronic cerebral hypoperfusion. *Neurobiol Aging*. **21**, 207-214.
47. Lee, P.H., Hwang, E.M., Hong, H.S., Boo, J.H., Mook-Jung, I. and Huh, K. (2006) Effect of ischemic neuronal insults on amyloid precursor protein processing. *Neurochem Res*. **31**, 821-827.
48. Zuroff, L., Daley, D., Black, K.L., and Koronyo-Hamaoui, M. (2017) Clearance of cerebral Aβ in Alzheimer's disease: reassessing the role of microglia and monocytes.*Cell Mol Life Sci*. **74(12),** 2167-2201.
49. Weller, R.O., Subash, M., Preston, S.D., Mazanti, I., and Carare, R.O. (2008) Perivascular drainage of amyloid-beta peptides from the brain and its failure in cerebral amyloid angiopathy and Alzheimer's disease. *Brain Pathol* **18(2)**, 253–266
50. Iliff, J.J., Wang, M., Liao, Y., Plogg, B.A., Peng, W., Gundersen, G.A., Benveniste, H., Vates, G.E., Deane, R., Goldman, S.A., Nagelhus, E.A., and Nedergaard, M. (2012) A paravascular pathway facilitates CSF flow through the brain parenchyma and the clearance of interstitial solutes, including amyloid beta. *Sci Transl Med* **4(147),** 147ra111.
51. Bordeleau, M., ElAli, A., and Rivest, S. (2016) Severe chronic cerebral hypoperfusion induces microglial dysfunction leading to memory loss in APPswe/PS1 mice. *Oncotarget.* **15;**7(11),11864-80.
52. Kövari, E., Gold, G., Herrmann, F.R., Canuto, A., Hof, P.R., Bouras, C. and Giannakopoulos, P. (2007) Cortical microinfarcts and demyelination affect cognition in cases at high risk for dementia. *Neurology*. **68**, 927-931.
53. Troncoso, J.C., Zonderman, A.B., Resnick, S.M., Crain, B., Pletnikova, O., and O'Brien, R.J. (2008) Effect of infarcts on dementia in the Baltimore longitudinal study of aging. *Ann Neurol*. **64**, 168-176.
54. Arvanitakis, Z., Leurgans, S.E., Barnes, L.L., Bennett, D.A. and Schneider, J.A. (2011) Microinfarct pathology, dementia, and cognitive systems. *Stroke*. **42**, 722-727.
55. Launer, L.J., Petrovitch, H., Ross, G.W., Markesbery, W. and White, L.R. (2008) AD brain pathology: vascular origins? Results from the HAAS autopsy study. *Neurobiol Aging*. **29**, 1587-1590.
56. Klein, W.L., Stine, W.B. Jr. and Teplow, D.B. (2004) Small assemblies of unmodified amyloid beta-protein are the proximate neurotoxin in Alzheimer's disease. *Neurobiol Aging*. **25**, 569-580.
57. Glabe, C.G. and Kayed, R. (2006) Common structure and toxic function of amyloid oligomers implies a common mechanism of pathogenesis. *Neurology*. **66**, S74–S78.
58. Haass, C. and Selkoe, D.J. (2007) Soluble protein oligomers in neurodegeneration: lessons from the Alzheimer's amyloid beta-peptide. *Nat.Rev.Mol.Cell Biol*. **8**, 101–112.
59. Walsh, D.M. and Selkoe, D.J. (2007) A beta oligomers - a decade of discovery. *J Neurochem*. **101**, 1172-1184.
60. Maezawa, I., Zimin, P.I., Wulff, H. and Jin, LW. Amyloid-beta protein oligomer at low nanomolar concentrations activates microglia and induces microglial neurotoxicity. *J Biol Chem*. **286**, 3693-3706 (2011).

Figure legends:

Figure 1. Parenchymal Aβ deposition following chronic cerebral hypoperfusion. There was no statistical difference in the % parenchymal Aβ at either 1 (a) or 3 months (b) after cerebral hypoperfusion compared to sham ($p > 0.05$). The data are presented as mean ± S.E.M. Representative images from sham and 3 months hypoperfused mice are shown which illustrate sections of the thalamus double immunostained with collagen (red) and Aβ (green). (scale bar = 50 μm).

Figure 2. Soluble Aβ levels are increased in response to cerebral hypoperfusion and precede insoluble Aβ accumulation in the parenchyma. The levels of soluble and insoluble Aβ40/42 were quantified in the parenchymal fraction by ELISA after 1 or three months sham or hypoperfusion. Graphs represent the levels of the protein normalized to total protein concentration. The data are presented as mean ± S.E.M.. After 1 month of hypoperfusion, significantly increased levels of both Aβ40 ($p = 0.02$) and Aβ42 ($p = 0.02$) were found in the soluble protein fraction, when compared to the sham control. In contrast, the insoluble protein fraction remained unchanged ($p > 0.05$). After 3 months of hypoperfusion, there were no significant changes between the sham and hypoperfused groups in the soluble fraction ($p > 0.05$), however increased concentration of both Aβ40 ($p = 0.002$) and Aβ42 ($p = 0.008$) was observed in the insoluble fraction.

Figure 3. Chronic cerebral hypoperfusion accelerates vascular amyloid. At one month there was no effect of hypoperfusion on vascular Aβ load (a) whereas at 3 months vascular Aβ load was significantly increased (b). The data are presented as mean ± S.E.M., $*p < 0.05$. Representative images from sham and 3 months hypoperfused mice are shown (scale bar = 50 μm). Double immunostaining was performed using markers of collagen (red) and Aβ (green). The arrows highlight amyloid localised to the vasculature.

Figure 4. Delayed accumulation of vascular Aβ in response to cerebral hypoperfusion. The levels of soluble and insoluble Aβ40/42 were quantified in the vessel-enriched fraction by ELISA after 1 or three months sham or hypoperfusion. Graphs represent the levels of the protein normalized to total protein concentration. The data are presented as mean ± S.E.M.. (a) There were no significant changes in the levels of soluble/insoluble Aβ40/42 determined

between hypoperfused and sham animals after 1 month of hypoperfusion ($p > 0.05$). (b) However, following 3 months there was a significant increase in the levels of both Aβ40 ($p = 0.002$) and Aβ42 ($p = 0.008$) in the insoluble fraction of the hypoperfused group compared to the sham animal but soluble levels of Aβ40/42 were unchanged ($p > 0.05$).

Figure 5. Chronic cerebral hypoperfusion increases APP levels and processing. Western blot analysis of brain protein extracts after 1 (a, c-e) and 3 (b, f-h) months of hypoperfusion was performed to determine the expression levels of full-length APP, CTFβ and CTFα. Specific bands were quantified by densitometric analysis and expressed relative to total tubulin protein, represented in the graphs. The data are presented as mean ± S.E.M., $p < 0.05$. There was a significant increase in the levels of APP ($p = 0.0008$), CTFβ ($p = 0.0002$) and CTFα ($p < 0.0001$) in the hypoperfused animals following 1 month when compared to the sham group (c-e); however, after 3 months of hypoperfusion no difference was observed between the two groups ($p > 0.05$, f-h)

Figure 6. Microinfarcts, associated with microglial proliferation, are precipitated by chronic cerebral hypoperfusion. Representative images showing normal (a) and infarcted (b) tissue using H&E staining. Iba1 staining was used to visualise microglial proliferation (c, d) (scale bar = 100 μm). Histopathological analysis was performed using H&E staining in tissue sections from Tg-SwDI and wild-type animals following 1 (e) and 3 (f) months of hypoperfusion; the area covered by infarcted tissue was measured and is represented in the graphs. The data are presented as mean ± S.E.M.. At one month there was a significant effect of genotype (***$p = 0.0005$). The area of infarct was significantly greater in hypoperfused Tg-SwDI mice compared to sham Tg-SwDI mice (*$p < 0.05$). At three months following hypoperfusion there was a significant effect of surgery (**$p = 0.003$) and genotype (***$p < 0.0001$), and furthermore there was a significant interaction (* $p = 0.03$) between surgery and genotype with a greater volume of infarct in hypoperfused Tg-SwDI mice (**$p < 0.01$).

Figure 7. Aβ increases NOX2 levels, which is exacerbated by chronic cerebral hypoperfusion. NOX2 levels were quantified in protein extracts from brain homogenate using ELISA after 1 (a) and 3 (b) months of hypoperfusion. Graphs represent the levels of the protein normalized to total protein concentration. The data are presented as mean ± S.E.M..

At one month, there was a significant effect of surgery ($F_{(1, 29)} = 4.29$, $p = 0.047$) and significant effect of genotype ($F_{(1, 29)} = 16.8$, $p = 0.0003$) on NOX2 levels but there was no significant interaction. Follow up post-hoc analysis indicated that NOX2 levels were significantly increased in Tg-SwDI hypoperfused mice compared to Tg-SwDI shams ($p < 0.05$) but there was no difference between wild-type sham and hypoperfused mice ($p > 0.05$) (Fig. 7a). At 3 months, there was no significant effect of surgery ($p < 0.05$) but there was a significant effect of genotype ($F_{(1, 23)} = 4.7$, $p = 0.04$) (Fig. 7b) and no significant interaction ($p > 0.05$). There was a positive correlation between NOX2 levels and soluble parenchymal Aβ40 levels, $r = 0.66$, $p = 0.002$ (c) and no correlation between NOX2 levels and vascular Aβ40 levels, $r = 0.085$, $p = 0.73$ (d).

Figure 8. Proposed mechanistic pathway for the contribution of chronic cerebral hypoperfusion to cognitive decline and mechanisms relevant to AD. Chronic cerebral hypoperfusion may initially increase the generation of soluble Aβ or Aβ oligomers that promote pro-inflammatory and oxidative stress mechanisms (such as NOX2) leading to degenerative changes such as microinfarcts. Over time Aβ may accumulate, particularly in the vasculature (CAA), exacerbating vascular dysfunction and accelerating degenerative changes and cognitive decline thus promoting a vicious cycle of events.

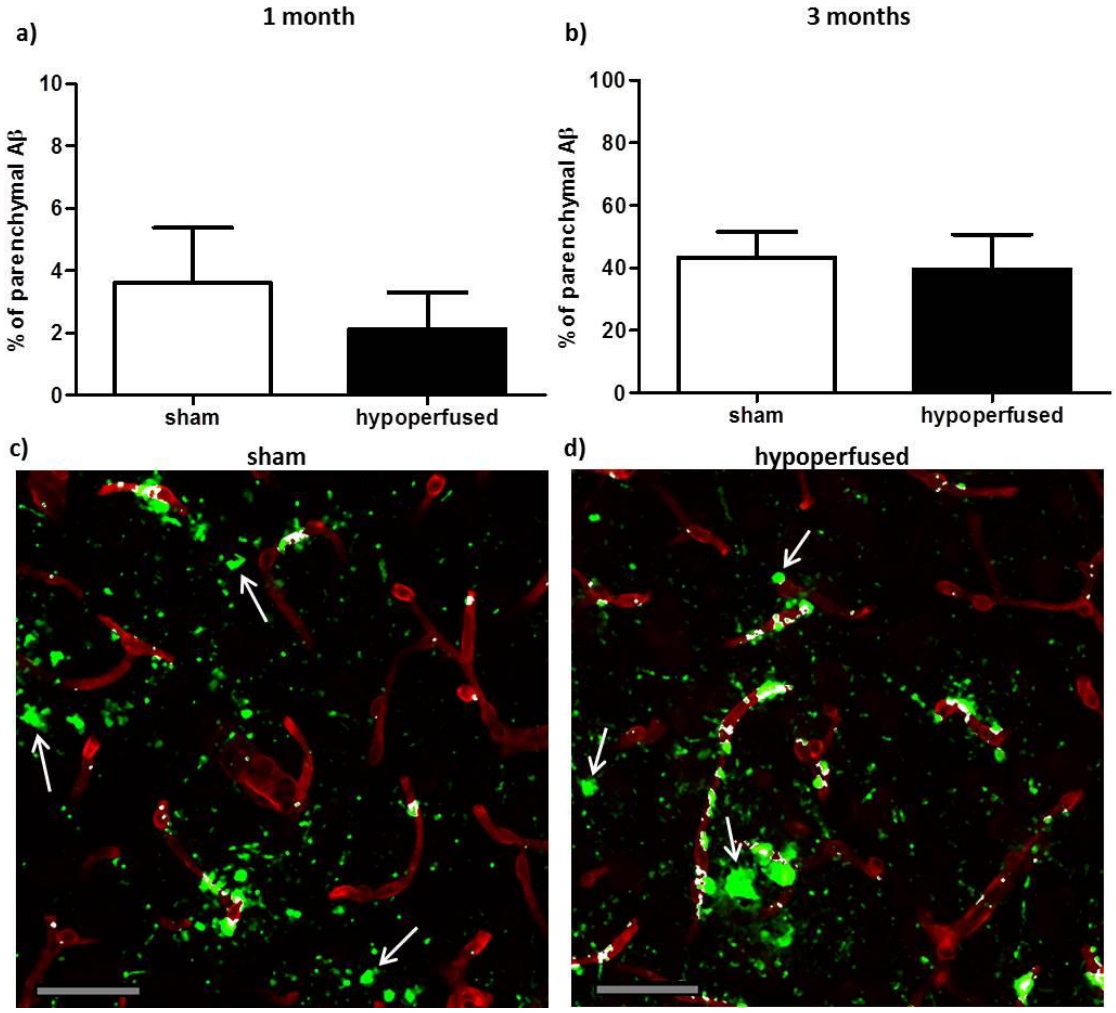
a)
1 month
% of parenchymal Aβ
10
8
6
4
2
0
sham
hypoperfused
b)
3 months
% of parenchymal Aβ
100
80
60
40
20
0
sham
hypoperfused
c)
sham
d)
hypoperfused

Figure 1

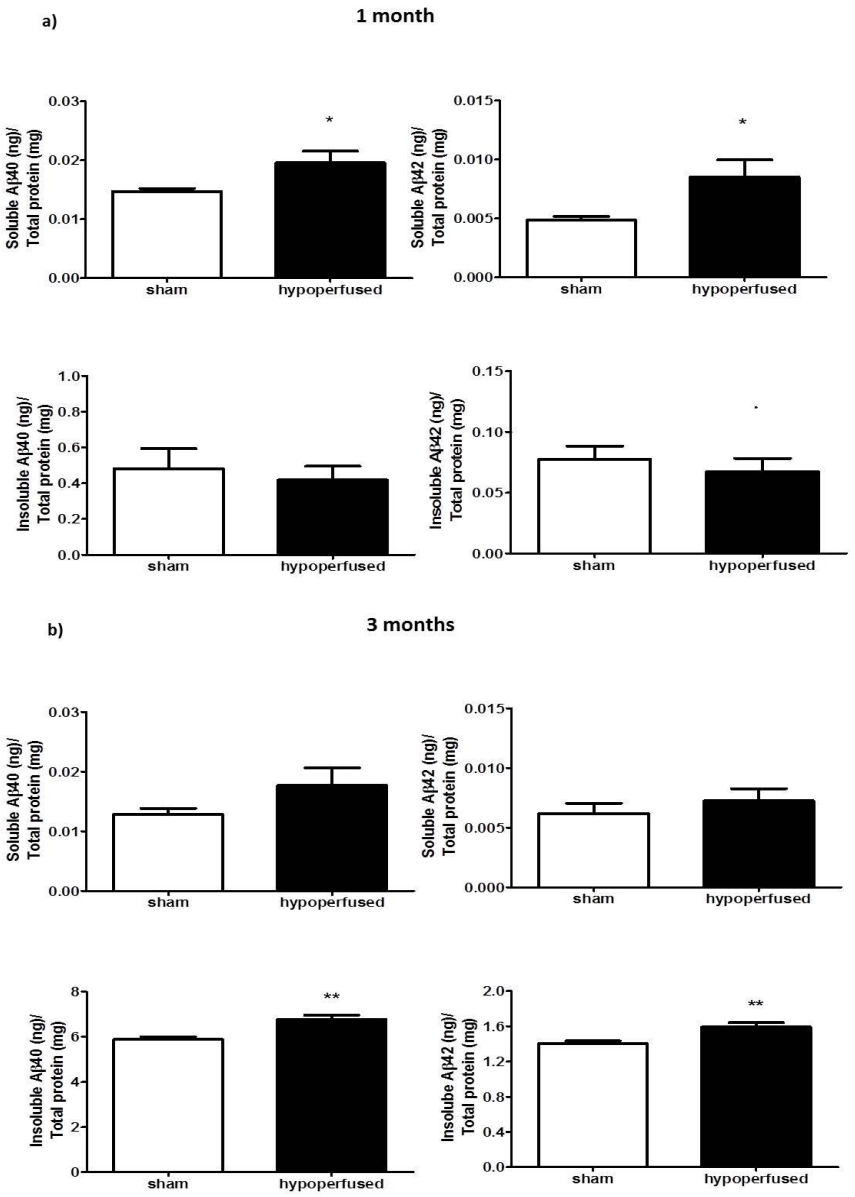
a)
1 month
Soluble Aβ40 (ng)/ Total protein (mg)
0.03
0.02
0.01
0.00
*
sham
hypoperfused
Soluble Aβ42 (ng)/ Total protein (mg)
0.015
0.010
0.005
0.000
*
sham
hypoperfused
Insoluble Aβ40 (ng)/ Total protein (mg)
1.0
0.8
0.6
0.4
0.2
0.0
sham
hypoperfused
Insoluble Aβ42 (ng)/ Total protein (mg)
0.15
0.10
0.05
0.00
sham
hypoperfused
b)
3 months
Soluble Aβ40 (ng)/ Total protein (mg)
0.03
0.02
0.01
0.00
sham
hypoperfused
Soluble Aβ42 (ng)/ Total protein (mg)
0.015
0.010
0.005
0.000
sham
hypoperfused
Insoluble Aβ40 (ng)/ Total protein (mg)
8
6
4
2
0
**
sham
hypoperfused
Insolube Aβ42 (ng)/ Total protein (mg)
2.0
1.6
1.2
0.8
0.4
0.0
**
sham
hypoperfused

Figure 2

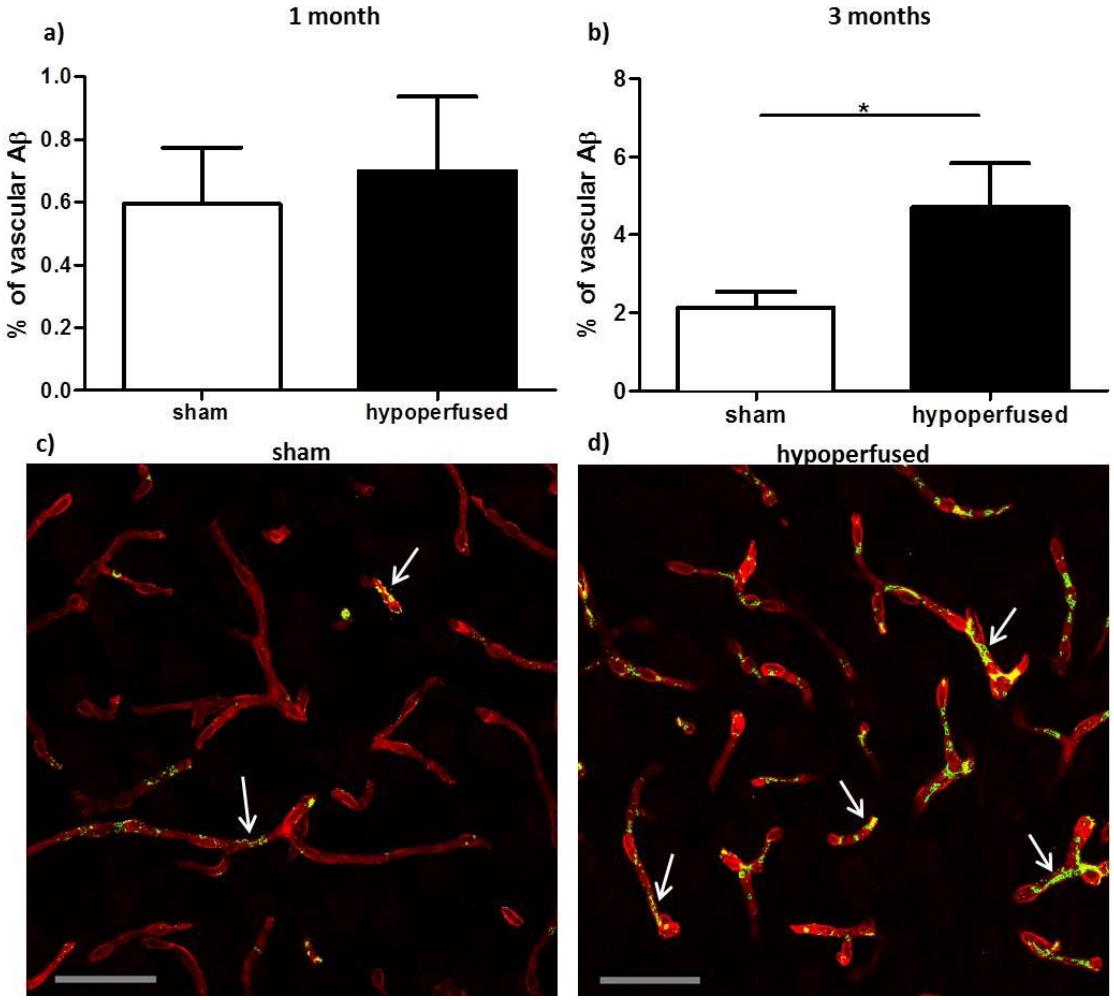
a)
1 month
% of vascular Aβ
1.0
0.8
0.6
0.4
0.2
0.0
sham
hypoperfused
b)
3 months
% of vascular Aβ
8
6
4
2
0
*
sham
hypoperfused
c)
sham
d)
hypoperfused

Figure 3

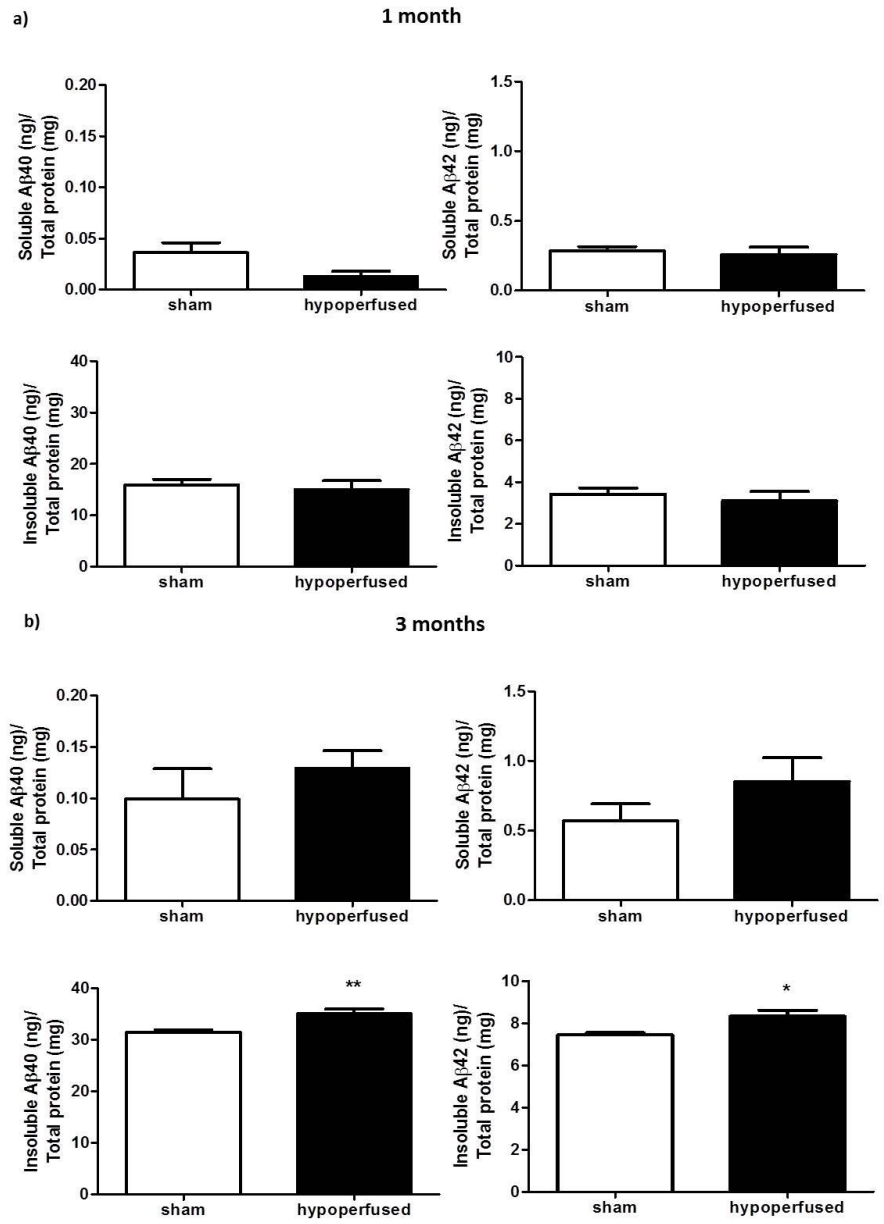
a)
1 month
Soluble Aβ40 (ng)/ Total protein (mg)
0.20
0.15
0.10
0.05
0.00
sham
hypoperfused
Soluble Aβ42 (ng)/ Total protein (mg)
1.5
1.0
0.5
0.0
sham
hypoperfused
Insoluble Aβ40 (ng)/ Total protein (mg)
40
30
20
10
0
sham
hypoperfused
Insoluble Aβ42 (ng)/ Total protein (mg)
10
8
6
4
2
0
sham
hypoperfused
b)
3 months
Soluble Aβ40 (ng)/ Total protein (mg)
0.20
0.15
0.10
0.05
0.00
sham
hypoperfused
Soluble Aβ42 (ng)/ Total protein (mg)
1.5
1.0
0.5
0.0
sham
hypoperfused
Insoluble Aβ40 (ng)/ Total protein (mg)
**
40
30
20
10
0
sham
hypoperfused
Insoluble Aβ42 (ng)/ Total protein (mg)
*
10
8
6
4
2
0
sham
hypoperfused

Figure 4

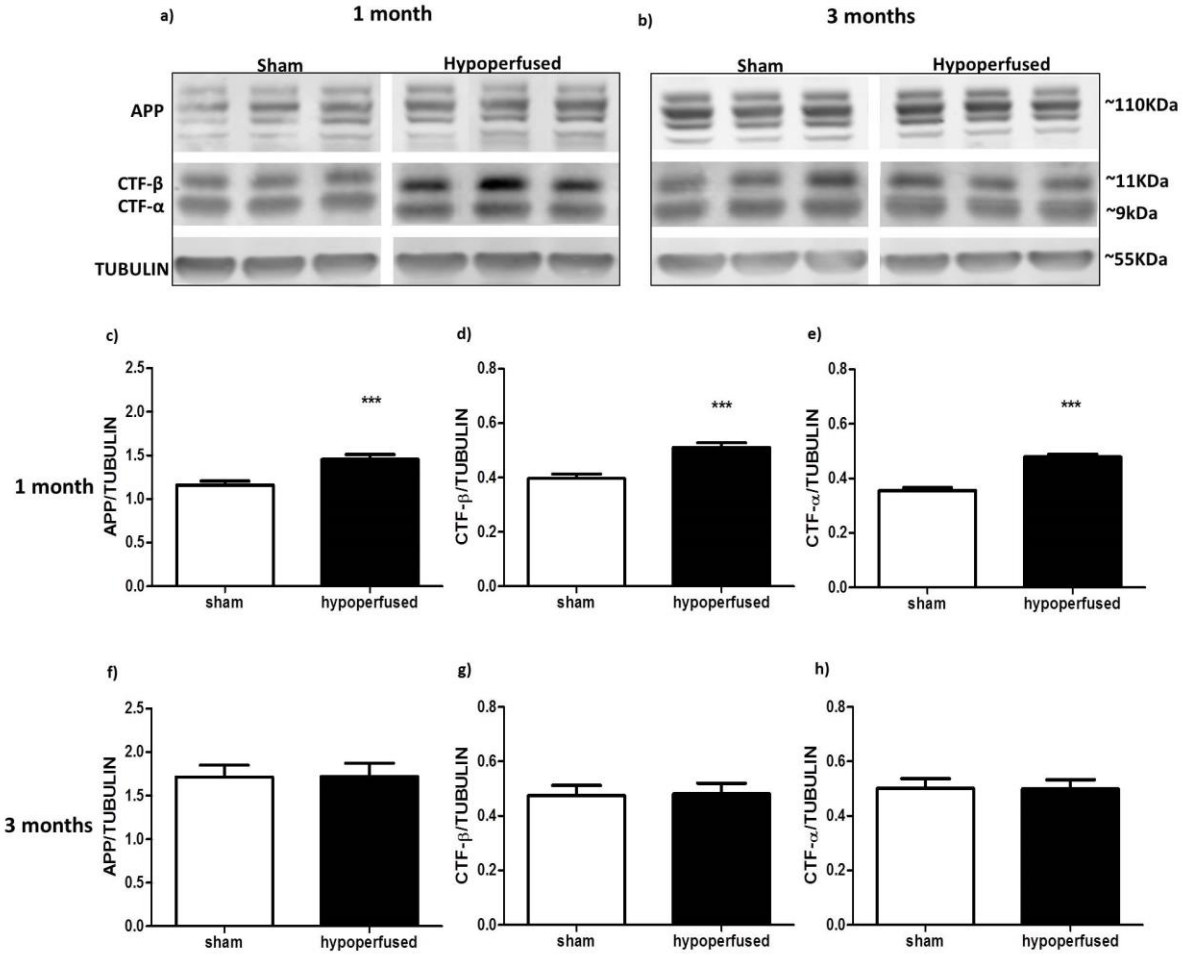
a)
1 month
Sham
Hypoperfused
APP
CTF-β
CTF-α
TUBULIN
b)
3 months
Sham
Hypoperfused
~110KDa
~11KDa
~9kDa
~55KDa
c)
d)
e)
1 month
APP/TUBULIN
CTF-β/TUBULIN
CTF-α/TUBULIN
***
sham
hypoperfused
f)
g)
h)
3 months
APP/TUBULIN
CTF-β/TUBULIN
CTF-α/TUBULIN
sham
hypoperfused

Figure 5

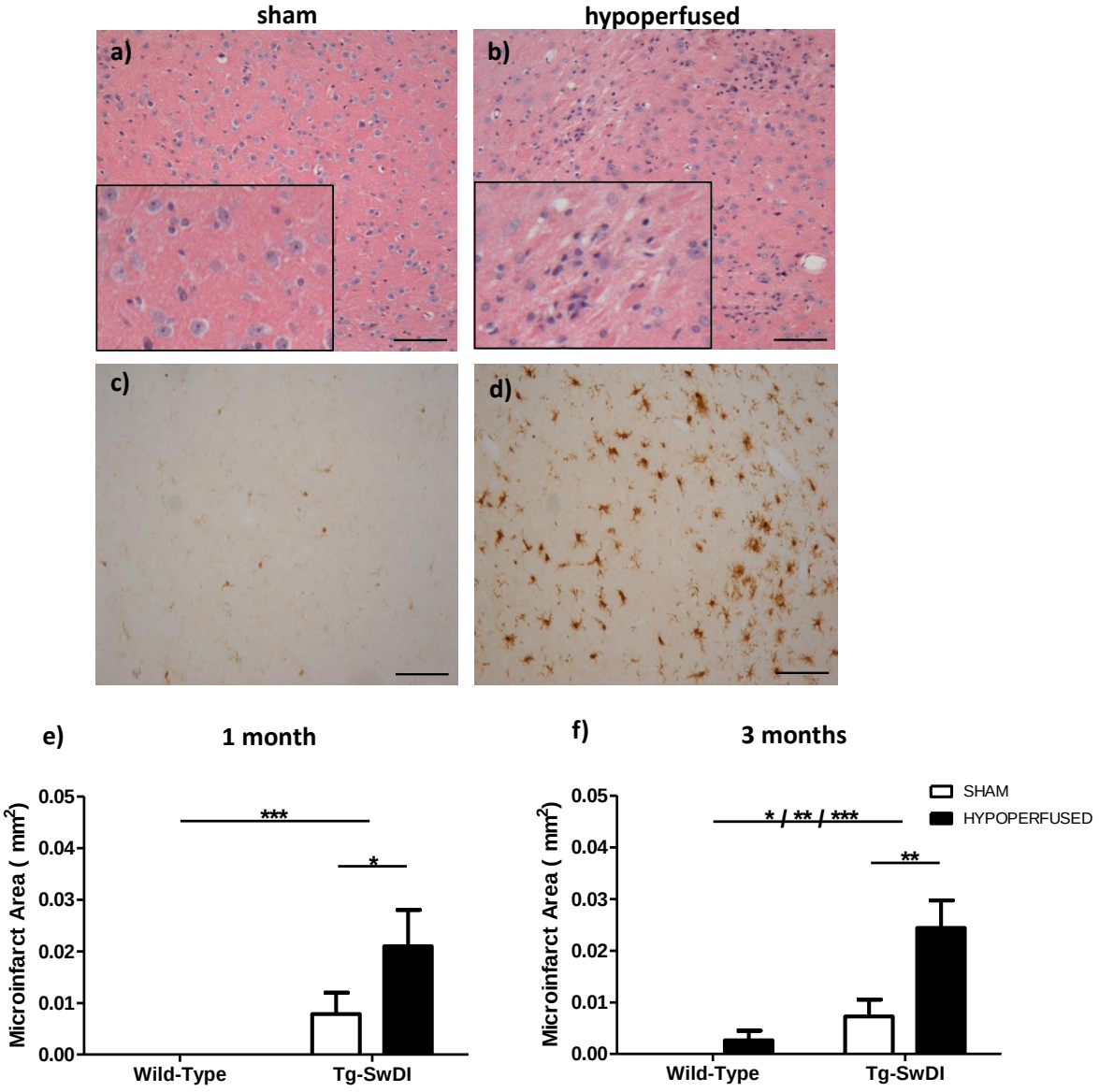
sham
hypoperfused
a)
b)
c)
d)
e)
1 month
f)
3 months
Microinfarct Area (mm2)
0.05
0.04
0.03
0.02
0.01
0.00
***
*
* / ** / ***
**
SHAM
HYPOPERFUSED
Wild-Type
Tg-SwDI

Figure 6

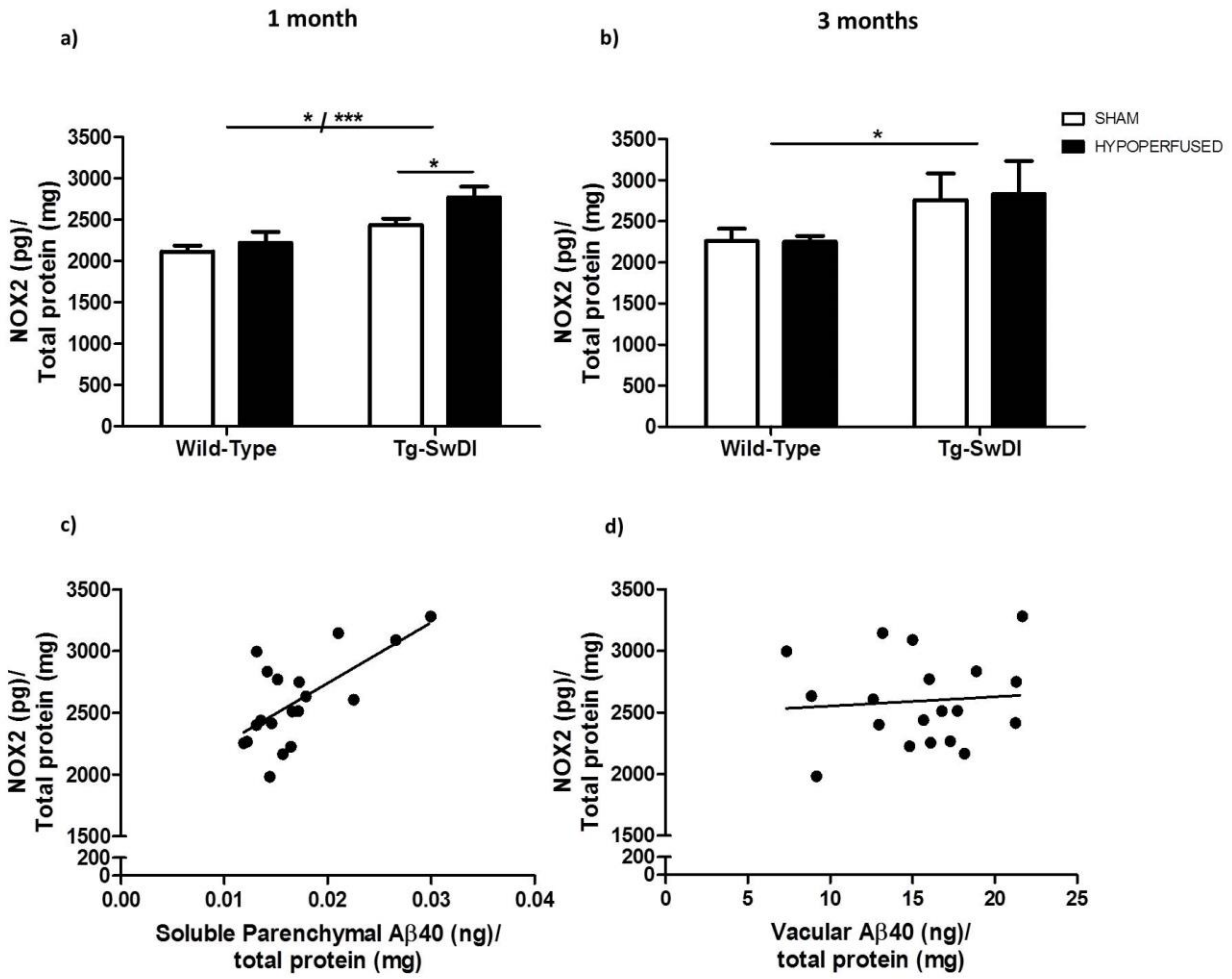
a)
1 month
* / ***
*
NOX2 (pg)/ Total protein (mg)
3500
3000
2500
2000
1500
1000
500
0
Wild-Type
Tg-SwDI
b)
3 months
*
SHAM
HYPOPERFUSED
c)
Soluble Parenchymal Aβ40 (ng)/ total protein (mg)
0.00
0.01
0.02
0.03
0.04
d)
Vacular Aβ40 (ng)/ total protein (mg)
0
5
10
15
20
25

Figure 7

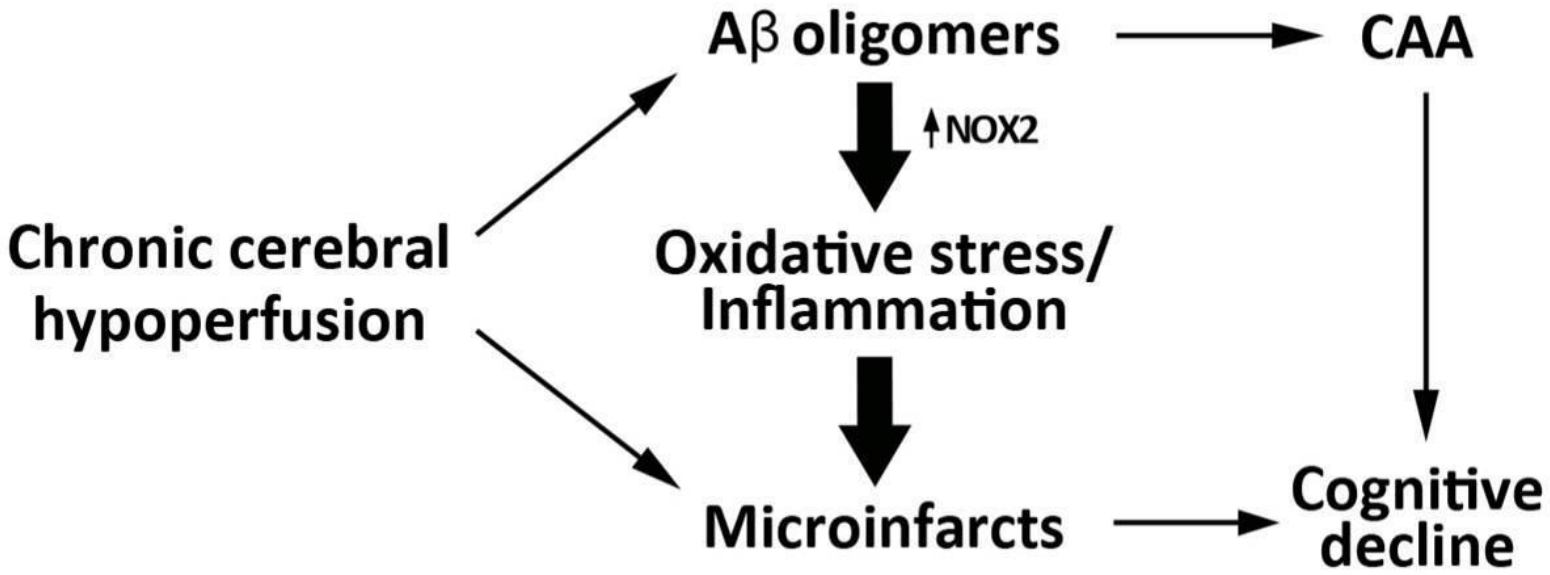
Aβ oligomers
CAA
NOX2
Chronic cerebral hypoperfusion
Oxidative stress/ Inflammation
Microinfarcts
Cognitive decline

Figure 8

Chronic cerebral hypoperfusion alters amyloid-β peptide pools leading to cerebral amyloid angiopathy, microinfarcts and haemorrhages in Tg-SwDI mice

Natalia Salvadores[1,2], James L. Searcy[1], Philip R. Holland[1,3], and Karen Horsburgh[1,4*]

[1]Centre for Neuroregeneration, University of Edinburgh, Chancellor's Building, 49 Little France Crescent. Edinburgh. EH164SB, UK.

[2]Center for Integrative Biology, Universidad Mayor, Chile

[3]Headache Group, Basic and Clinical Neuroscience, Institute of Psychiatry, Psychology and Neuroscience, King's College London, London, UK.

[4]Centre for Cognitive Ageing and Cognitive Epidemiology, University of Edinburgh, 7 George Square, Edinburgh, EH89JZ, UK.

*corresponding author karen.horsburgh@ed.ac.uk

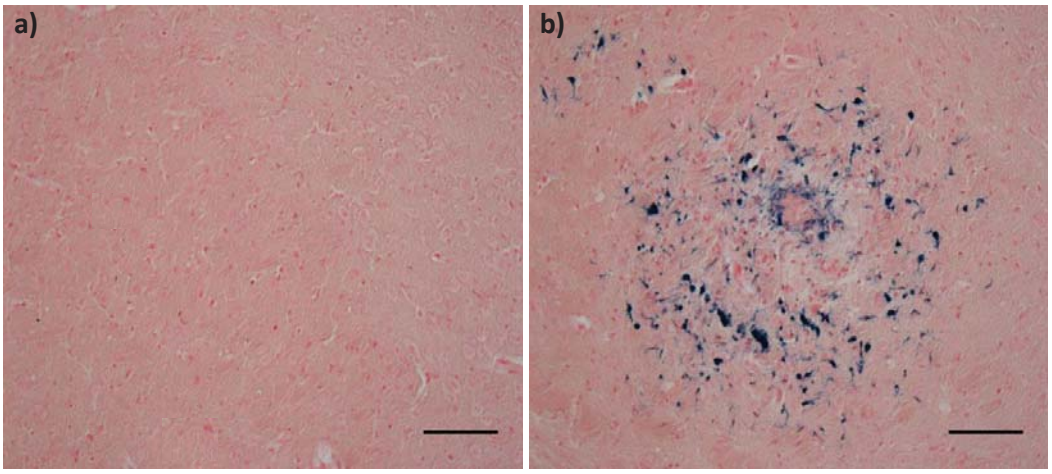

c)

	1 month		3 months	
	sham	hypoperfused	sham	hypoperfused
Wild-Type	0/12 (0%)	0/11 (0%)	0/10 (0%)	1/10 (10%)
Tg-SwDI	0/9 (0%)	0/10 (0%)	0/9 (0%)	3/9 (33%)

Figure S1. Proportion of mice with thalamic hemorrhages following chronic cerebral hypoperfusion. Histopathological analysis was performed using Perls staining in tissue sections from Tg-SwDI and wild-type animals following 1 and 3 months of hypoperfusion. Representative images showing normal (a) and hemorrhagic (b) tissue are shown (scale bar = um). The number of mice with thalamic hemorrhages was determined and is indicated in the table.